Electrochimica Acta 71 (2012) 173–180

Contents lists available at SciVerse ScienceDirect

Electrochimica Acta

journal homepage: www.elsevier.com/locate/electacta

# Mesoporous Pt electrocatalyst for methanol tolerant cathodes of DMFC

Esteban A. Franceschini[a], Mariano M. Bruno[a,b], Federico A. Viva[a], Federico J. Williams[c], Matías Jobbágy[c], Horacio R. Corti[a,c,*]

[a] Comisión Nacional de Energía Atómica (CNEA), Departamento de Física de la Materia Condensada, Centro Atómico Constituyentes, Av. General Paz 1499 (1650), San Martín, Buenos Aires, Argentina
[b] Escuela de Ciencia y Tecnología, Universidad de Gral. San Martín, Martín de Irigoyen 3100 (1650), San Martín, Buenos Aires, Argentina
[c] Instituto de Química Física de los Materiales, Medio Ambiente y Energía (INQUIMAE-CONICET), Facultad Ciencias Exactas y Naturales, Universidad de Buenos Aires, Pabellón 2, Ciudad Universitaria, C1428GA, Buenos Aires, Argentina

ARTICLE INFO

*Article history:*
Received 14 September 2011
Received in revised form 22 January 2012
Accepted 26 March 2012
Available online 4 April 2012

*Keywords:*
Fuel cells
Mesoporous Pt
Oxygen
Electroreduction
Methanol

ABSTRACT

High activity mesoporous Pt electrocatalyst, having 2D-hexagonal mesostructure, was synthesized using a triblock poly(ethylene oxide)-b–poly(propylene oxide)-b–poly(ethylene oxide) copolymer (Pluronic F127®) template. The catalyst was characterized for the oxygen reduction reaction (ORR) in a rotating ring disk electrode (RRDE) configuration, obtaining a high efficiency of conversion to $H_2O$. The formation of $H_2O_2$ during the ORR was low and a change in Tafel slope analysis indicated a change in the reaction mechanism with temperature. It was found, through differential electrochemical mass spectrometry (DEMS) analysis, that the mesoporous Pt catalysts exhibit a high methanol to $CO_2$ conversion efficiency and high tolerance to CO poisoning. The procedure described in this work for preparing mesoporous Pt catalyst by electrodeposition provides a simple method for the generation of high-performance cathodes for direct methanol PEM fuel cells.



## 1. Introduction

The electrochemical oxygen reduction reaction (ORR) has been extensively studied in relation to its role as controlling process in determining the efficiency of the electrochemical conversion in PEM fuel cells [1–5]. The reaction mechanism in both, acidic and alkaline solutions, has been widely investigated [6,7], and the effect of numerous parameters, such as pH [6,7], pre-treatment of the electrode [6], type of electrolytes [6–9], electrolyte concentrations [9,10], temperature [10], exposed crystalline facets of the catalysts [11,12] and particle size [13] on the reaction kinetics have been examined.

Several mechanisms have been reported in the literature for the electroreduction of oxygen on platinum electrodes surface, most of them showing a parallel production of $H_2O$ and $H_2O_2$ [14–16]. Despite that the ORR is a multi-electron charge transfer reaction proceeding via several elementary steps, it can be analyzed on the basis of the simple model proposed by Damjanovic et al. [14]. This model states that the ORR in aqueous solution can occur via two pathways mechanism indicated in the scheme below: (i) direct four electron reduction to water (pathway 1), and (ii) series reactions (pathway 2) involving $H_2O_2$ as intermediate.

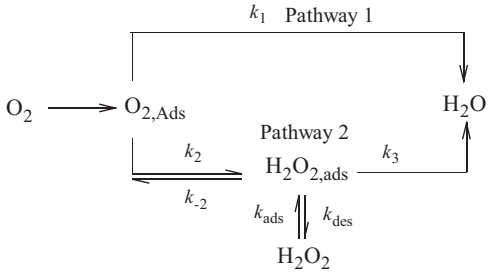


In the proposed mechanisms $k_1$ is the rate constant of the direct oxygen reduction reaction (via 4 electrons), $k_2$ and $k_3$ are the rate constants for the oxygen reduction series reaction (via consecutive 2 electrons transfer steps), and $k_{ads}$ and $k_{des}$ are the kinetics constants of adsorption and desorption of $H_2O_2$ over the catalyst surface, having a direct relation with the $H_2O_2$ yield.

The catalyst efficiency toward the formation of $H_2O_2$ (or $H_2O$) can be quantified employing an electrode rotator in a Rotating Disk Electrode (RDE) and Rotating Ring Disk Electrode (RRDE) techniques [17–19], and their use assumes three statements: (i) absence of catalytic decomposition of $H_2O_2$; (ii) the adsorption/desorption equilibrium of $H_2O_2$ is rapidly reached; (iii) the rate constant for the $H_2O_2$ oxidation ($k_{-2}$) is negligible.

The sluggishness of the ORR is one of the main causes for PEM fuel cells not reaching higher efficiencies. In direct methanol PEM fuel cells (DMFC) there is also the problem of the methanol

* Corresponding author at: Comisión Nacional de Energía Atómica (CNEA), Departamento de Física de la Materia Condensada, Av. General Paz 1499 (1650), San Martín, Buenos Aires, Argentina. Tel.: +54 11 67727174; fax: +54 11 67727121.
*E-mail address:* hrcorti@cnea.gov.ar (H.R. Corti).

0013-4686/$ – see front matter © 2012 Elsevier Ltd. All rights reserved.
http://dx.doi.org/10.1016/j.electacta.2012.03.121

crossover from anode to cathode, which produces a decrease in the cell performance due to parasitic oxidation current and the blocking of catalytic sites due to CO formation [20–22].

Different strategies were adopted in order to overcome this drawback. For instance, it is well known [23–25] that different crystalline Pt facets have characteristic poisoning resistances to CO, as well as adsorption energies for oxygenated species (i.e., OH, $H_2O$), a fact that can be used to maximize the catalysts CO poisoning resistance, as well as optimize its catalytic activity toward the ORR. As a matter of fact, Pt nanoparticles exhibit different exposed crystallographic planes depending of their sizes [26], and the understanding of the structure–catalytic activity relationship of mesoporous Pt catalysts is a key factor on the development of new catalysts with higher activities and utilization degrees.

Research in materials for electro-catalysis commonly focuses on reducing the noble metal loading, with the addition of a second or third metal in the form of an alloy. The addition of transition metals such as Fe, Ni, Co, and Ru were explored [27–29], but these metals are very unstable under the highly oxidant environment of a DMFC cathode with acid electrolyte. Although a large number of binary and ternary alloys [19,30–32] have been tested, metallic Pt is currently the most widely used cathodic electrocatalyst in fuel cells fed with air or oxygen [33,34].

The methods used to obtain structures with relatively well-defined crystal planes are generally expensive and structures with low electrochemical area are obtained. The use of block copolymers allows obtaining well defined mesoporous structures in a simple and reproducible way, leading to unusual catalytic properties, such as lower poisoning rates and higher conversion efficiencies than nanoparticled catalysts [35], which could be even increased by the addition of a second or third metal [35,36].

The purposes of this work are: (i) to synthesize a mesoporous Pt catalyst, employing Pluronic F127 as patterning agent, a procedure which is simpler than other methods for preparing mesoporous catalysts, because it is performed at room temperature, and it does not require stabilization times to obtain an ordered structure as liquid crystals templates [35]; (ii) to compare the catalytic activity for the ORR and the $H_2O$ yield of the mesoporous Pt catalyst with other nanostructured catalysts. At the same time, we will study the efficiency of the cathodic electrocatalyst under methanol crossover conditions, that is, toward $CO_2$ production and catalyst poisoning.

## 2. Experimental

### 2.1. Chemicals

Triblock poly(ethylene oxide)-b–poly(propylene oxide)-b–poly(ethylene oxide) copolymer $EO_{106}PO_{70}EO_{106}$, denoted Pluronic F127® ($M_w$ = 12.600, Aldrich), hydrated hexachloroplatinic acid (HCPA, 99.99%, Aldrich), methanol (99.8%, Research S.A.) and sulfuric acid (PA grade, Research S.A.) were used as received. All aqueous solutions were prepared with deionized water having resistivity ≈18 MΩ cm, and degassed using high purity $N_2$ (Indura S.A.). High purity $O_2$ (Indura S.A.) gas was used for the electrochemical experiments.

### 2.2. Preparation of mesoporous platinum catalysts

The mesoporous Pt catalyst was deposited on gold by electrochemical reduction of a mixture of 0.2 M aqueous solution of HCPA and 50 wt.% aqueous solution of Pluronic F127, following the method described in a previous work [35]. The viscous mixture was poured in a purpose-built three-electrode electrochemical cell having a gold disk working electrode, a Pt wire as counter electrode, and a Ag/AgCl(sat) reference electrode. The platinum was reduced applying a current of 0.2 mA $cm^{-2}$ for 30 min.

### 2.3. Morphological characterization

Scanning Tunneling Microscopy (STM) images were acquired with a Veeco-DI Multimode Nanoscope IIIa, with 10 μm lateral scan range and a 2 μm z-scanner. The bias potential was fixed at 10 mV and the tunneling current at 1 nA, employing a Pt/Ir tip (Nano Devices, Veeco Metrology, Santa Barbara, CA).

Field Emission Scanning Electron micrographs were obtained using a Supra 40 (Zeiss Company) FESEM operating at a voltage of 3 kV, equipped with an Oxford EDX.

X-ray Photoelectron Spectroscopy (XPS) measurements were performed under UHV conditions (base pressure $<5 \times 10^{-10}$ mbar) in a SPECS UHV spectrometer system equipped with a 150 mm mean radius hemispherical electron energy analyzer and a nine channeltron detector. XPS spectra were acquired at a constant pass energy of 20 eV using an unmonochromated Mg Kα (1253.6 eV) source operated at 12.5 kV and 20 mA and a detection angle of 30° with respect to the sample normal on grounded conducting substrates. Quoted binding energies are referred to the adventitious C 1s emission at 285 eV.

Powder X-ray diffraction (PXRD) patterns were obtained with a SIEMENS D-5000 instrument, employing Ni-filtered Cu Kα radiation. PXRD patterns were recorded between 30° and 90°, employing a 0.02° step size and a 4 s step time. Eventual pattern displacements were corrected employing the peaks of a gold substrate as reference. Pt diffraction peaks were deconvoluted from the substrate ones by means of Profile fitting software.

### 2.4. Electrochemical characterization

All electrochemical experiments were performed employing an Autolab PGSTAT302N potentiostat (Echochemie, Netherlands). For RRDE experiments the Autolab potentiostat was coupled to a rotating ring disk electrode (Pine Research Inst.; Raleigh, NC). A Saturated Calomel Electrode (SCE) was used for all the electrochemical experiments and the potentials in this work were referred to the Reference Hydrogen Electrode (RHE). The counter electrode was a large area rolled platinum wire (0.5 mm in diameter, 30 cm length). A three electrodes electrochemical cell with a jacket was employed, and its temperature was controlled by circulating a thermostatized liquid using a Techne temperature controller. Purpose built three electrodes electrochemical cells were employed in the mesoporous catalyst synthesis and DEMS analysis.

#### 2.4.1. Electrochemical surface area (ECSA)

Cyclic voltammetric measurements were carried out in 0.5 M $H_2SO_4$ at 298 K in order to analyze the $H_2$ adsorption/desorption peaks areas, cycling between 0 and 0.9 V (vs. RHE). The charge was integrated between 0 and 0.4 V and the double layer charge was discounted using the conventional method [37].

#### 2.4.2. Oxygen reduction analysis by RDE and RRDE

Oxygen reduction experiments were performed using a rotating gold disk electrode (0.196 $cm^2$) – platinum ring electrode (Pine Research Inst.). RDE and RRDE measurements were performed in the temperature range from 293 K to 313 K, in 0.5 M $H_2SO_4$ aqueous media, and efficiency parameters were calculated by means of Tafel's plots. Voltammograms were recorded for the ORR at different rotation speed ($\omega$ = 100–2500 rpm). The potential was scanned between 1.1 and 0 V (vs. RHE) at 10 mV $s^{-1}$. The calibration of the RRDE was carried out by measuring the disk and ring currents in a 0.005 M $K_3Fe(CN)_6$ + 0.1 M $K_2SO_4$ electrolyte. The disk potential

was cycled between 0.0 and 1.0 V at 10 mV $s^{-1}$ while the ring potential was fixed at 1.4 V in order to oxidize the $Fe^{+3}$ generated in the disk. This procedure was repeated at different rotating speed. The RRDE collection efficiency ($N$) was determined from the slope of disk current ($I_D$) vs. ring current ($I_R$) plots [38,39].

*2.4.3. Methanol oxidation analysis by DEMS*

The methanol oxidation reaction (MOR) was investigated in order to assess the tolerance of the catalyst in the case of methanol crossover, when used in a DMFC. DEMS analysis was conducted in order to obtain the methanol to $CO_2$ ($m/z = 44$) conversion efficiency at 298 K. The experiments were carried out in a flow electrochemical cell designed particularly for DEMS similar to the one used by Pastor et al. [40]. The working electrode used was a gold disk built ad hoc (0.283 $cm^2$) with a 0.1 mm in diameter hole in the center used to allow the reactant flow during the measurement. The flow rate (0.4 ml $min^{-1}$) was controlled by resorting to the hydrostatic pressure of the electrolyte in the reservoir, using a two-chamber flow system.

The calculation of the efficiency for methanol conversion to $CO_2$ by DEMS requires a previous determination of the $m/z = 44$ calibration constant, $K(44)$ by means of a procedure described in detail in numerous publications [20,40–42], which involves the measurement of the Faradaic charge, $Q_F^{CO}$, corresponding to the oxidation of CO to $CO_2$. The CO voltammetric striping experiments were performed in 0.5 M $H_2SO_4$ solution at 298 K holding the electrode potential at 250 mV (vs. RHE) during 1 h. The potential was then scanned between 50 and 850 mV (vs. RHE) in the anodic direction, at 1 and 5 mV $s^{-1}$. $K(44)$ is calculated through the expression:

$$K(44) = \frac{2Q_{MS}(44)}{Q_F^{CO}} \quad (1)$$

where $Q_{MS}(44)$ is the integrated mass spectrometric current for $CO_2$ and 2 is the number of electrons for the electro-oxidation of CO to $CO_2$.

The average current efficiency of the methanol electro-oxidation to $CO_2$ was calculated using the following equation [43]:

$$\eta_Q = \frac{Q_F^*}{Q_F^{CH_3OH}} \quad (2)$$

where $Q_F^{CH_3OH}$ is the total Faradaic charge (i.e., forward and reverse scan charge) and $Q_F^*$ is the Faradaic charge corresponding to the formation of $CO_2$, given by:

$$Q_F^* = \frac{6Q_{MS}(44)}{K(44)} \quad (3)$$

where 6 is the number of electrons involved in the methanol oxidation to $CO_2$, and $Q_{MS}(44)$ is the integrated mass spectrometric current of the $CO_2$ generated by methanol oxidation, measured in one potential sweep cycle as an average of the cathodic and the anodic sweep over all the potential range.

## 3. Results and discussion

### 3.1. Morphological analysis

#### 3.1.1. STM

STM characterization was carried out in order to elucidate the morphology of the electrodeposits at nanometric scale. Fig. 1 shows that the catalyst structure is formed by an array of spheres resulting in a hexagonal pore arrangement, as showed in a previous work [35]. The image analysis indicates that the mean particle size is approximately 9 nm and, considering the proposed hexagonal arrangement, it is expected that the pore size is the same order of particle size [35].

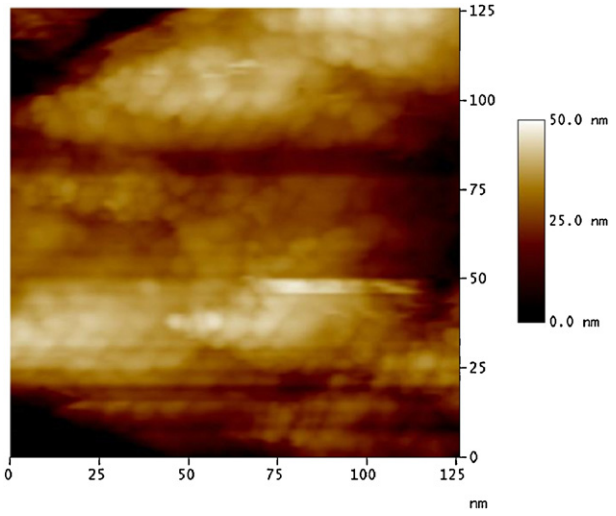


**Fig. 1.** STM image (125 × 125 × 50) nm of the electrodeposited mesoporous Pt catalyst.

#### 3.1.2. FESEM

High-resolution electron micrographs were acquired in order to confirm the presence of a mesoporous structure in the catalyst. As shown in Fig. 2, the catalyst layers are formed by porous spheres having 40–60 nm in diameter and a pore diameter of ~9 nm in size (measured directly from the FESEM image). This structure is consistent with the STM analysis (Fig. 1) and with the results of our previous work [35].

#### 3.1.3. XPS

Survey XPS scans show the presence of Pt and the expected C and O contamination with no other elements being observed on the fresh catalyst. Thus XPS confirms the absence of metallic impurities. Fig. 3 shows the XPS spectrum corresponding to the Pt 4*f* region, which consists of the expected doublet with binding energies of 71.2 eV (Pt $4f_{7/2}$) and 74.5 eV (Pt $4f_{5/2}$). The binding energy position reflects the oxidation state of platinum and it corresponds to metallic Pt. The presence peaks at binding energies greater than 72 eV, corresponding to Pt oxides (Pt $4f_{7/2}$), are clearly negligible and therefore it can be ruled out.

In summary, the XPS analysis shows a mesoporous film composed by pure metallic Pt with no oxide present.

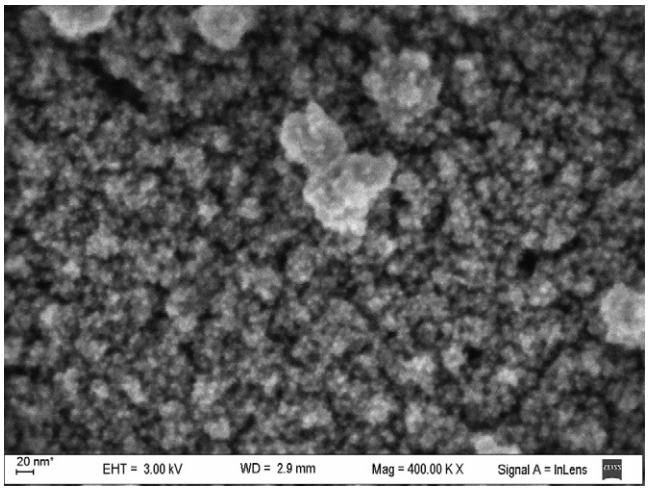


**Fig. 2.** FESEM micrograph of mesoporous Pt catalyst. Magnification: 400,000×.

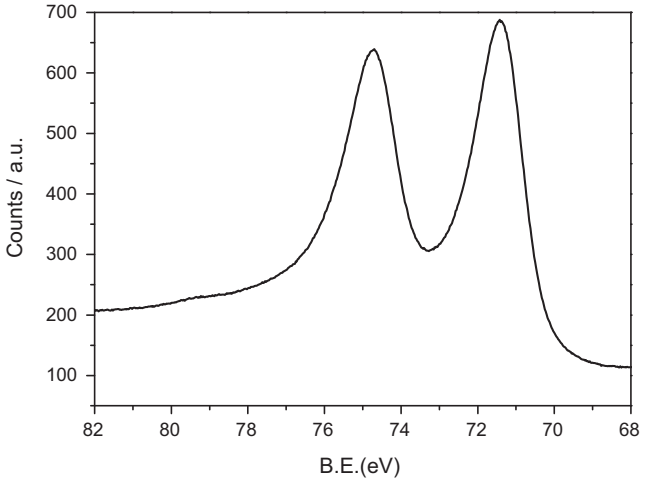


**Fig. 3.** Pt 4*f* XP spectra of the mesoporous Pt thin film.

### 3.1.4. XRD

The X-ray diffractograms of mesoporous Pt catalyst are shown in Fig. 4. The Pt phase cell parameter was $0.392 \pm 0.001$ nm, in good agreement with bibliography [44]. An average crystal size of $9 \pm 1$ nm was calculated using Scherrer's equation [45–47], which is consistent with the STM measurements.

## 3.2. Electrochemical characterization

### 3.2.1. Hydrogen adsorption–desorption

The catalysts exhibit well-defined $H_2$ adsorption/desorption peaks in the potential region 0–300 mV (vs. RHE), after 10 cycles between 0 and 950 mV (vs. RHE) at 100 mV $s^{-1}$ (Fig. 5a). The electrochemical active surface areas of the catalysts were calculated using the integrated charge in the $H_2$ adsorption/desorption region, and for all the electrodes used in the present work (ORR and MOR experiments) the obtained values were in the range of 23–25 $m^2\,g^{-1}$, which is consistent with the results of our previous work [35].

### 3.2.2. ORR analysis by RDE

The overall measured current density, *j*, of the oxygen reduction can be expressed in terms of the kinetic current density, $j_k$, and the

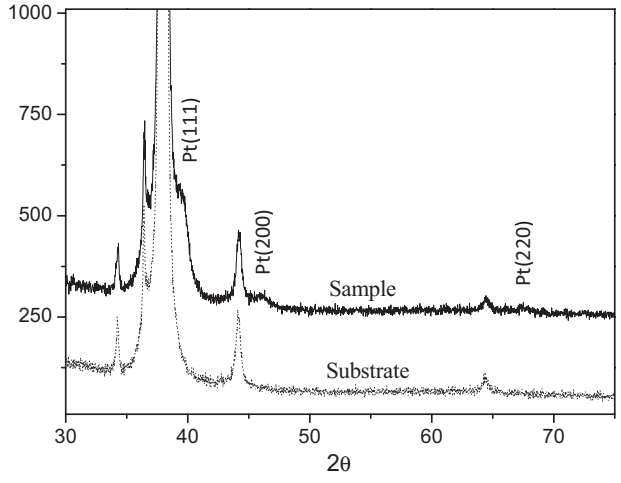


**Fig. 4.** XRD patterns of mesoporous Pt deposited onto Au substrate (filled line) and bare Au substrate (dotted line). Main diffraction peaks related to Pt crystalline structure.

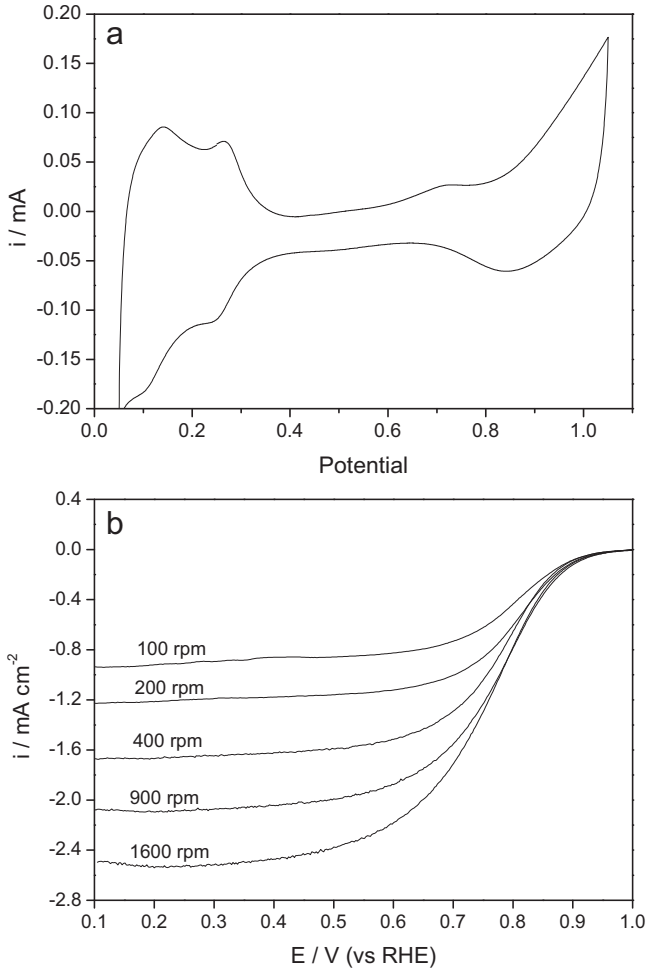


**Fig. 5.** (a) Cyclic voltammetry of mesoporous platinum in 0.5 M $H_2SO_4$ at 298 K; (b) Current–potential curves obtained in 0.5 M $H_2SO_4$ for ORR on mesoporous Pt at different rotation rates.

diffusion limited current density, $j_d$, by the Koutecky–Levich (KL) equation [48]:

$$\frac{1}{j} = \frac{1}{j_k} + \frac{1}{j_d} = \frac{1}{j_k} + \frac{1}{B\omega^{1/2}} \quad (4)$$

*B* being,

$$B = 0.2nFC_O{D_O}^{2/3}\nu^{-1/6} \quad (5)$$

where 0.2 is a constant used when the rotation speed, $\omega$ is expressed as rpm, *n* is the number of electrons transferred per molecule of $O_2$ reduced, *F* the Faraday constant, $C_O$ is the concentration of oxygen dissolved ($1.1 \times 10^{-6}$ mol $cm^{-3}$), $D_O$ is the diffusion coefficient of oxygen in the solution ($1.4 \times 10^{-5}$ $cm^2\,s^{-1}$) [49], and $\nu$ the kinematic viscosity of the 0.5 M $H_2SO_4$ solution ($1.0 \times 10^{-2}$ $cm^{-2}\,s^{-1}$) [49], all of them at 298 K. It is possible to calculate the theoretical slope of the KL plot ($\log j$ vs. $\omega^{-1/2}$) considering a four electrons process, i.e., a complete reduction of $O_2$ to $H_2O$. The dependences of the oxygen concentration and diffusion coefficient with temperature were taken into account for corrections of the theoretical 4 electrons K–L plots using the values reported in literature [50].

Fig. 5b shows a set of RDE current density–potential curves, obtained in $O_2$ saturated 0.5 M $H_2SO_4$ at 293 K, which exhibit a well defined charge-transfer kinetic control, mixed kinetic-diffusion, and diffusion-limited currents. A similar behavior was found for the density–potential curves measured at other temperatures.

The slopes of the KL plot (not showed) allow us to calculate the number of electrons involved in the ORR. The

**Table 1**
Kinetics parameters calculated from the Tafel slope for the ORR on mesoporous Pt catalysts in 0.5 M $H_2SO_4$ solution.

| Temperature (K) | $j_0$ (mA cm$^{-2}$) | Tafel slope (mV dec$^{-1}$) |
|---|---|---|
| 293 | $2.8 \times 10^{-5}$ | −95 |
| 298 | $1.2 \times 10^{-4}$ | −106 |
| 303 | $4.1 \times 10^{-4}$ | −121 |
| 308 | $6.3 \times 10^{-4}$ | −124 |
| 313 | $2.6 \times 10^{-3}$ | −152 |

theoretical calculated slope (considering a 4 electrons process), was $9.41 \times 10^{-2}$ mA$^{-1}$ cm$^2$ rpm$^{1/2}$ at 298 K, while the experimental slope observed for mesoporous Pt was close to $9.45 \times 10^{-2}$ mA$^{-1}$ cm$^2$ rpm$^{1/2}$. The measured KL slope yields $n = 3.98$ (considering a transfer coefficient $\alpha = 0.5$), leading to the conclusion that the ORR on mesoporous Pt catalyst follows a 4 electrons charge transfer process to water formation. We will validate this conclusion by RRDE analysis, vide infra.

Tafel analysis was also performed at temperatures between 293 and 313 K, in order to obtain information of the reduction mechanism in mesoporous Pt through Tafel slope ($b$) and exchange current density ($j_0$). Usually, Tafel plots for the ORR on platinum electrodes show different well-defined slopes, at low and high current densities. In general, the slope at low current densities (related to the transfer of 2 electrons) is constant with temperature, and Tafel slopes are analyzed at high current densities (related to the transfer of 4 electrons). Tafel parameters at high current densities are summarized in Table 1. The exchange current density, $j_0$, was evaluated as a function of temperature, taking into consideration the reversible oxygen electrode potential, $E_r$, at each temperature. The dependence of $E_r$ on temperature was evaluated using the Nernst equation, $E_r = -\Delta G^0_{(H_2/O_2)}/2F$, with the following temperature dependence [39] for $\Delta G^0_{(H_2O_2)}$:

$$\Delta G^0_{(H_2/O_2)}(\text{Jmol}^{-1}) = -296,658 - 33.6T \ln T + 389.8T \quad (6)$$

As can be seen in Table 1, both, $b$ and $j_0$, varies with the temperature. The behavior of $b$ is consistent with a possible change in the reaction mechanism [51,52], which could be caused by changes in the adsorption geometry of oxygen species on the catalyst surface [16], leading to a variation in the $H_2O_2$ yield [16]. The increase of $j_0$ with temperature has been widely reported in the literature [18,19].

### 3.2.3. ORR analysis by RRDE

The RRDE analysis allows us to calculate the $H_2O_2$ percentage generated during the $O_2$ reduction, through pathway 2, using the equation [53]:

$$\%H_2O_2 = \frac{200 I_R/N}{I_D + I_R/N} \quad (7)$$

where $N$ is the experimental collection efficiency which corresponds to the $I_R/I_D$ ratio ($N = 0.18$).

Fig. 6a depicts the disk and the ring currents vs. the disk potential obtained in RRDE experiments for the mesoporous Pt catalyst. The electrochemical behavior of the ring currents, associated with the $H_2O_2$ oxidation, dependent on the rotation rate at the scanned potentials. According to Damjanovic et al. [14] the relationship between the disk and ring currents provides information on the influence of the different reaction pathways in the overall reaction mechanism. The $I_D/I_R$ vs. $\omega^{-1/2}$ plot (Fig. 6b) seems to validate a mechanism where the 4 electrons direct formation of $H_2O$, and the 2 electrons consecutive reactions, via the $H_2O_2$ intermediary, occurs simultaneously.

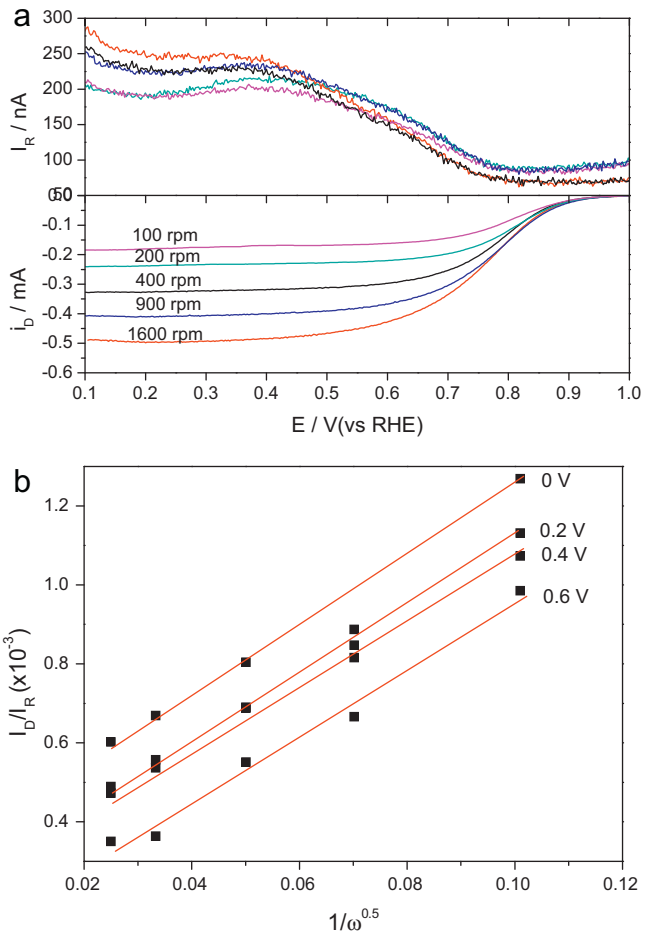


**Fig. 6.** (a) Steady-state polarization curves at different rotation rates for ORR on mesoporous Pt disk and Pt ring held at 1.4 V (vs. RHE). Sweep rate: 5 mV s$^{-1}$; (b) $I_D/I_R$ vs. $\omega^{-1/2}$ plot.

The percentage of $H_2O_2$ produced as a function of the electrode disk potential at different electrode rotation speeds is shown in Fig. 7a measured at 298 K. The maximum quantity of $H_2O_2$, between 0.5% and 1.4% depending on the rotation speed, forms at 0.35–0.45 V (vs. RHE). This result indicates that, at 298 K, the ORR proceed mostly to water, with a yield of ~99%, following preferentially a 4 electron transfer reaction mechanism, but, although the production of $H_2O_2$ is low, is not negligible and presents a clear dependence on the applied potential. Fig. 7b shows that the efficiency toward $H_2O_2$ increases with increasing the temperature. This can be indicative of a change in the kinetic parameters with temperature favoring pathway 2, where the intermediate $H_2O_2$ is released into the solution before the formation of $H_2O$ takes place. This change in the kinetics parameters is consistent with the Tafel slope change observed (see Table 1). The variation in the $H_2O_2$ yield with temperature turns impossible the calculation of the transfer coefficient, because the change in $n$ cannot be decoupled from the transfer coefficient, since the transfer coefficient calculation requires the value of n remains constant with temperature.

The conversion efficiencies of the ORR toward $H_2O_2$ reported for several catalysts at 298 K, 0.4 V, and at different rotating rates [54–58], are summarized in Table 2. It can be seen that the mesoporous Pt catalyst synthesized via electrodeposition with F127® shows a lower production of $H_2O_2$ over the entire range of studied rotation speeds. This finding could be explained considering that the structure of a nanoparticulated catalyst would allows a relatively simple way of releasing $H_2O_2$, diffusing away from

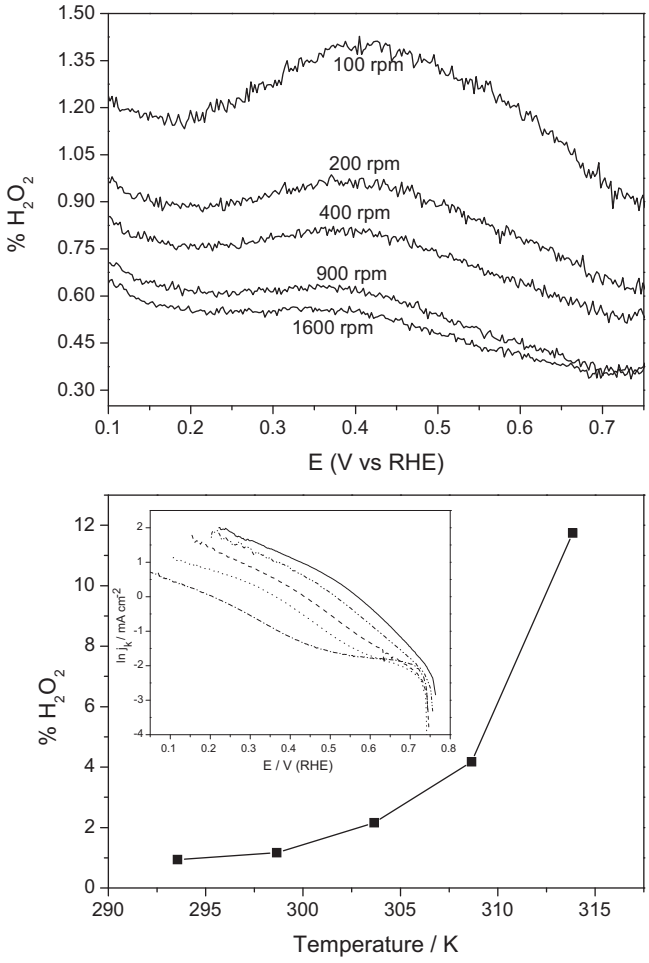


**Fig. 7.** (a) Percentage of $H_2O_2$ produced as function of the disk potential at different rotating rates (298 K); (b) Percentage of $H_2O_2$ produced as function of the temperature at 200 rpm and 0.4 V (vs. RHE). Inset in (b) Tafel plots for mesoporous Pt at different temperatures; 293 K (—), 298 K (-·-·-), 303 K (—), 308 K (···) and 313 K (-·-).

the surface of the catalyst. This effect would be diminished in a mesoporous catalyst due to confinement effects that increase the probability of readsorption of $H_2O_2$, improving the efficiency of $H_2O$ production.

### 3.2.4. MOR analysis by DEMS

DEMS analysis was carried out in order to analyze the efficiency of the methanol oxidation toward $CO_2$ on mesoporous Pt catalyst. It is known that a low conversion efficiency of methanol to $CO_2$ implies a high production of intermediates, like HCOOH and CO. In particular, CO is adsorbed strongly on the Pt surface, blocking the catalytic sites and decreasing the catalyst efficiency.

Fig. 8a shows the CO strip, carried out in order to obtain the cell constant $K(44) \approx 2.5 \times 10^{-5}$, where a well-defined peak with an onset at ~0.5 V vs. RHE, that is a typical value for Pt under these conditions, can be observed. CVs for methanol electrooxidation in 1 M $CH_3OH$ + 1 M $H_2SO_4$ solution at 298 K are shown in Fig. 8b, along with the corresponding mass signals for $CO_2$ ($m/z$ = 44) and formic acid followed through methylformate formation ($m/z$ = 60) during methanol electrooxidation at 298 K.

The averaged conversion efficiency of methanol to $CO_2$ of 51% was obtained from the anodic and cathodic scans. This percentage is similar to that obtained by Wang et al. [43] for Pt/C (50%, w/w) under similar conditions, and ~10% higher than the obtained for Pt/C (20%, w/w). Moreover, the obtained efficiency is 10–20% higher than that reported for a mesoporous Pt catalysts with a smaller pore diameter (2–3 nm) [40]. This indicates that the oxidation of methanol is more efficient on the surface of the mesoporous catalyst obtained via Pluronic F127 template than other platinum based catalysts (like nanoparticulated and mesoporous catalysts with smaller pore diameter) with a lower formation of CO, which in turns diminishes the possibility of catalyst poisoning.

**Table 2**
Comparison of $H_2O_2$ (RRDE) and $CO_2$ (DEMS) conversion efficiencies of different catalysts.

| Catalyst | rpm | % $H_2O_2$ | Ref |
|---|---|---|---|
| RRDE | | | |
| NP Mo–Ru–Se | 100–1000 | 2.6–3 | [54] |
| NP W–Se–$Os(CO)_n$ | 100–900 | 2.5–2.9 | [55] |
| NP Pt/C (20%, w/w) | 2400 | 3–3.5 | [56] |
| NP RuWSe | 3500 | 2 | [57] |
| NP RuMoSe | Not informed | 1.9 | [58] |
| MP Pt | 100–1600 | 0.55–1.4 | This work |

| Catalyst | $CH_3OH$ conc (M) | Flow (ml $min^{-1}$) | Eff (%) | Ref |
|---|---|---|---|---|
| DEMS | | | | |
| PC Pt | 0.1–0.2 | 0.1–1.8 | 25.3–40.5 | [59]* |
| PC Pt, $Pt_{(111)}$, $Pt_{(332)}$ | 0.1 | 0.3 | 20–28 | [60] |
| NP Pt/C 40%, w/w | 0.1–0.001 | 0.3 | 30–48 | [61]* |
| MP Pt | 1 | 0.4 | 31 | [52] |
| MP Pt/Ru | 1 | 0.4 | 20 | [52] |
| MP PtRu (decorated) | 1 | 0.4 | 37 | [52] |
| PC Pt | 0.2 | 0.6 | ~20 | [43]* |
| NP Pt/C 50%, w/w Etek | 0.2 | 0.6 | ~50 | [43]* |
| NP Pt/C 20%, w/w Etek | 0.2 | 0.6 | ~35 | [43]* |
| MP Pt | 1 | 0.4 | 51 | This work |

All the reported values were obtained at a scan rate of 10 mV $s^{-1}$, except [52] (20 mV $s^{-1}$), and at 298 K, except those indicated with (*), reported as "room temperature". MP, mesoporous; NP, nanoparticulated, PC, polycrystalline. PC catalysts correspond to bulk materials.

The results of methanol to $CO_2$ conversion efficiency for catalysts with different morphology (nanoparticulated, mesoporous and polycrystalline bulk), and different compositions (Pt and PtRu) [43,52,59–61], are compared in Table 2 with that obtained for the mesoporous Pt catalyst prepared in this work. It is worthy to note that the mesoporous catalysts synthesized via Pluronic F127® exhibits higher efficiency of methanol oxidation toward $CO_2$ than the mesoporous PtRu catalysts reported in the literature, even when Ru is added with the aim of improve the $CO_{ads}$ tolerance of the Pt based catalysts.

It can be also seen in Table 2 that the mesoporous Pt prepared in this work has a similar conversion efficiency than the nanoparticulated catalysts with a high Pt loading (NP Pt/C 40–50%, w/w). This result could be explained considering that the nanoparticulated catalysts with high loading contain bigger particles than the nanoparticulated catalysts with low loadings [62,63], which enhances the possibility of having well-defined crystal planes [64]. Furthermore, the mesoporous catalysts synthesized via Pluronic F127® exhibits higher efficiency of methanol oxidation than mesoporous catalysts with lower pore diameter. As argued above, this could be explained by both, the presence of better defined crystal planes in the Pluronic F127® mesoporous catalyst, and the confinement effects, which could prevent the proper reaction of methanol, as proposed in a previous work [35].

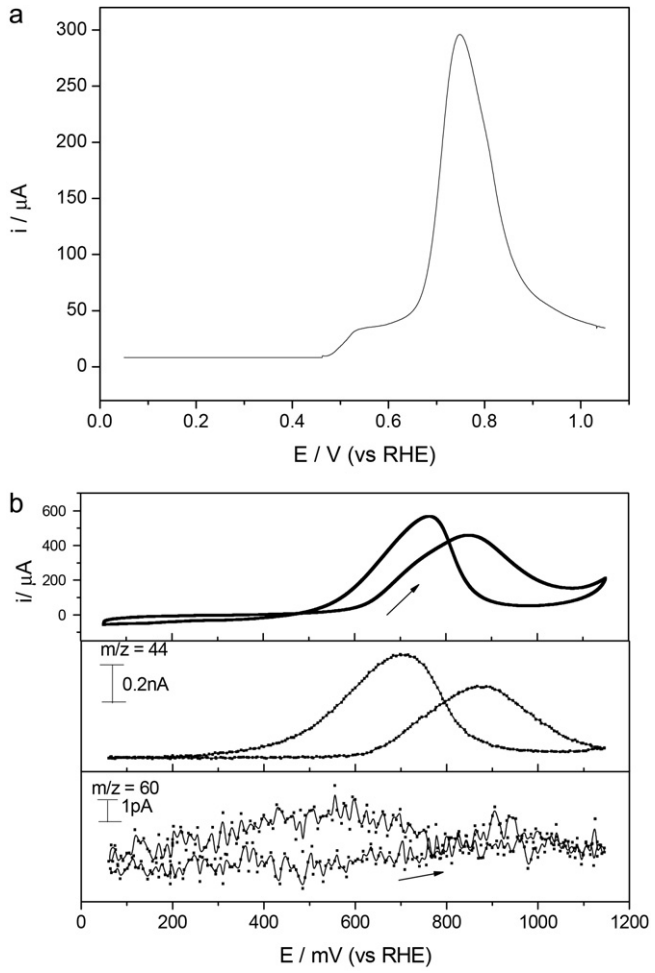


**Fig. 8.** (a) Anodic CV for $CO_{ads}$ oxidation on mesoporous Pt; (b) CVs and MSCVs for $CO_2$ ($m/z = 44$) and $HCO_2H$ ($m/z = 60$) formed during methanol electrooxidation of 1 M $CH_3OH$/1 M $H_2SO_4$ on Pt(65)Ru(35) at 298 K. Scan rate: 5 mV $s^{-1}$.

## 4. Conclusions

The procedure described in this work for preparing mesoporous Pt catalyst by electrodeposition, using Pluronic F127 block copolymer as template, provides a method for the generation of high-performance cathodes for DMFC. This mesoporous Pt catalysts exhibits a high oxygen conversion degree toward $H_2O$, which seem also indicate, a low $H_2O_2$ production, an undesired secondary product in the cathode of PEM fuel cells.

It was shown that mesoporous Pt catalyst synthesized using Pluronic F127 shows a lower $H_2O_2$ production over the entire range of studied rotation speeds. Furthermore, the mesoporous Pt catalyst was also found to have higher conversion efficiencies of methanol to $CO_2$ than mesoporous Pt catalysts with smaller pore diameter, but similar to some conventional nanosized catalysts supported on carbon substrates.

The preponderance of (1 1 1) crystalline planes, that could not be corroborated in the XRD analysis due to the small particle size, would explain the high efficiency to form $CO_2$ from methanol, because this plane hinders the formation of $CO_{ads}$ [25].

The increase in the amount of $H_2O_2$ with increasing temperature, taking into account the mechanism considered, could be due to both, an increase of $k_{des}$ and a decrease of $k_1$. In this case, changes in kinetic and transfer coefficient, and the number of electrons transferred per molecule of $O_2$, as evidenced by the change in efficiency of $H_2O_2$ formation make impossible a reliable calculation of the kinetics parameters of the mechanisms. The mesoporous catalysts synthesized via Pluronic F127 exhibit a high $CO_2$ efficiency even with concentrated methanol solutions. The large mesopore size and structural surface of our mesoporous Pt catalysts might help preventing the CO poisoning, maintaining the catalyst surface accessible to the oxygen, as we proposed in a previous work [35].

In summary, the Pt catalyst studied in this work is easy to synthesize, and have high conversion efficiencies and catalytic activities compared to other Pt catalyst with similar mesoporous structure, and even with Pt nanoparticles supported on carbon.

## Acknowledgments

The authors thank financial support from Agencia Nacional de Promoción Científica y Tecnológica (PICT 2097, PAE 36985), and CONICET (PIP 00095). H.R.C., M.M.B., F.A.V., F.J.W., and M.J. are permanent research fellows of CONICET. E.A.F. thanks CONICET for a graduate fellowship.

## References

[1] G. Faubert, D. Guay, J.P. Dodelet, Journal of the Electrochemical Society 145 (1998) 2985.
[2] M. Eikerling, A.A. Kornyshev, Journal of Electroanalytical Chemistry 453 (1998) 89.
[3] S. Fukada, Energy Conversion and Management 42 (2001) 1121.
[4] A.K. Shukla, M. Neergat, P. Bera, V. Jayaram, M.S. Hegde, Journal of Electroanalytical Chemistry 504 (2001) 111.
[5] E.H. Yu, K. Scott, R.W. Reeve, Fuel Cells 4 (2003) 169.
[6] A. Damjanovic, V. Brusic, Electrochimica Acta 12 (1967) 615.
[7] D.B. Sepa, M.V. Vojnovic, A. Damjanovic, Electrochimica Acta 26 (1981) 781.
[8] K.L. Hsueh, E.R. Gonzalez, S. Srinivasan, Electrochimica Acta 28 (1983) 691.
[9] K.L. Hsueh, E.R. Gonzalez, S. Srinivasan, D.T. Chin, Journal of the Electrochemical Society 131 (1984) 823.
[10] S.M. Park, S. Ho, S. Aruliah, M.F. Weber, C.A. Ward, R.D. Venter, S. Srinivasan, Journal of the Electrochemical Society 133 (1986) 1641.
[11] V. Tripković, E. Skúlason, S. Siahrostami, J.K. Nørskov, J. Rossmeisl, Electrochimica Acta 55 (2010) 7975.
[12] V. Stamenkovic, B.S. Mun, K.J.J. Mayrhofer, P.N. Ross, N.M. Markovic, J. Rossmeisl, J. Greeley, J.K. Norskov, Angewandte Chemie: International Edition 45 (2006) 2897.
[13] J.P. Greeley, J. Rossmeisl, A. Hellman, J.K. Nørskov, Zeitshrift fur Physikalische Chemie 221 (2007) 1209.
[14] A. Damjanovic, M.A. Geshav, J.O.'M. Bockris, Journal of Chemical Physics 45 (1966) 4057.
[15] J.K. Norskov, J. Rossmeisl, A. Logadottir, L. Lindqvist, J.R. Kitchin, T. Bligaard, H. Jónsson, Journal of Physical Chemistry B 108 (2004) 17886.
[16] K.C. Pillai, J.O.'M. Bockris, Journal of the Electrochemical Society 131 (1984) 568.
[17] D.B. Sepa, M.V. Vojnovic, L.M. Vracar, A. Damjanovic, Electrochimica Acta 29 (1984) 1169.
[18] R.G. Gonzalez-Huerta, A.R. Pierna, O. Solorza-Feria, Journal of New Materials for Electrochemical Systems 11 (2008) 63.
[19] K. Suárez-Alcántara, O. Solorza-Feria, Fuel Cells 10 (2010) 84.
[20] V.A. Paganin, E. Sitta, T. Iwasita, W. Vielstich, Journal of Applied Electrochemistry 35 (2005) 1239.
[21] C. Deryn, S. Gilman, Journal of the Electrochemistry Society 141 (1994) 1770.
[22] Z. Qi, A. Kaufman, Journal of Power Sources 110 (2002) 177.
[23] E. Herrero, K. Franaszczuk, A. Wieckowsk, Journal of Physical Chemistry 98 (1994) 5074.
[24] H.C. Wang, S. Ernst, H. Baltruschat, Physical Chemistry Chemical Physics 12 (2010) 2190.
[25] J.X. Wang, N.M. Markovic, R.R. Adzic, Journal of Physical Chemistry B 108 (2004) 4127.
[26] F. Raimondi, G.G. Scherer, R. Kötz, A. Wokaun, Angewandte Chemie: International Edition 44 (2005) 2.
[27] C. Roth, N. Martz, H. Fuess, Physical Chemistry Chemical Physics 3 (2001) 315.
[28] H. Yang, C. Coutanceau, J.M. Léger, N. Alonso-Vante, C. Lamy, Journal of Electroanalytical Chemistry 576 (2005) 305.
[29] V. Baglio, A.S. Arico, A. Stassi, C. D'Urso, A. Di Blasi, A.M. Castro Luna, V. Antonucci, Journal of Power Sources 159 (2006) 900.
[30] P. Sotelo-Mazón, R.G. Gonzalez-Huerta, J.G. Cabañas-Moreno, O. Solorza-Feria, International Journal of the Electrochemistry Society 2 (2007) 523.
[31] L. Zhang, K. Lee, J. Zhang, Electrochimica Acta 52 (2007) 7964.
[32] G. Ramos-Sánchez, A.R. Pierna, O. Solorza-Feria, Journal of Non-Crystalline Solids 354 (2008) 5165.
[33] A. Chen, P. Holt-Hindle, Chemical Reviews 110 (2010) 3767.
[34] H.A. Gasteiger, S.S. Kocha, B. Sompalli, F.T. Wagner, Applied Catalysis B: Environmental 56 (2005) 9.

[35] E.A. Franceschini, G.A. Planes, F.J. Williams, G.J.A.A. Soler-Illia, H.R. Corti, Journal of Power Sources 196 (2011) 1723.
[36] A. Kucernak, J. Jiang, Chemical Engineering Journal 93 (2003) 81.
[37] S. Trasatti, O.A. Petrii, Pure and Applied Chemistry 63 (1991) 711.
[38] O. Solorza-Feria, S. Ramírez-Raya, R. Rivera-Noriega, E. Ordoñez-Regil, S.M. Fernández-Valverde, Thin Solid Films 311 (1997) 164.
[39] K. Suárez-Alcántara, A. Rodríguez-Castellanos, R. Dante, O. Solorza-Feria, Journal of Power Sources 157 (2006) 114.
[40] E. Pastor, G.A. Planes, G. García, Electrochemistry Communications 9 (2007) 839.
[41] Z. Jusys, J. Kaiser, R.J. Behm, Langmuir 19 (2003) 6759.
[42] H. Baltruschat, Journal of the American Society for Mass Spectrometry 15 (2004) 1693.
[43] H. Wang, L.R. Alden, F.J. DiSalvo, H.D. Abruña, Langmuir 25 (2009) 7725.
[44] A.S. Arico, P.L. Antonucci, E. Modica, V. Baglio, H. Kim, V. Antonucci, Electrochimica Acta 47 (2002) 3723.
[45] W.Z. Li, W.Z. Zhou, H.Q. Li, Z.H. Zhou, B. Zhou, G.Q. Sun, Q. Xin, Electrochimica Acta 49 (2004) 1045.
[46] Z.Q. Tian, S.P. Jiang, Y.M. Liang, P.K. Shen, Journal of Physical Chemistry B 110 (2006) 5343.
[47] Z. Hou, B. Yi, H. Yu, Z. Lin, H.J. Zhang, Journal of Power Sources 123 (2003) 116.
[48] A.J. Bard, L. Faulkner, Electrochemical Methods 2nd ed., John Wiley & Sons, NY, USA, 2001.
[49] C. Couteanceau, P. Crouigneau, J.M. Léger, C. Lamy, Journal of Electroanalytical Chemistry 389 (1994) 379.
[50] D.R. Lide, Handbook of Chemistry and Physics, 79th ed., CRC Press, 1998.
[51] S.J. Clouser, J.C. Huang, E. Yeager, Journal of Applied Electrochemistry 23 (1993) 597.
[52] L.B. Kriksunov, Electrochimica Acta 40 (1995) 2553.
[53] H.A. Gasteiger, W. Gu, R. Makharia, M.F. Mathias, B. Sompalli, in: W. Vielstich, H.A. Gasteiger, A. Lamm (Eds.), Handbook in Fuel Cell, vol. 3, John Wiley & Sons, Chicester, West Sussex, United Kingdom, 2003.
[54] N. Alonso-Vante, H. Tributsch, O. Solorza-Feria, Electrochimica Acta 40 (1995) 567.
[55] R.H. Castellanos, A. Campero, O. Solorza-Feria, International Journal of Hydrogen Energy 23 (1998) 1037.
[56] R. Benitez, A.M. Chaparro, L. Daza, Journal of Power Sources 151 (2005) 2.
[57] K. Suarez-Alcantara, O. Solorza-Feria, Fuel Cells 10 (2010) 84.
[58] K. Suarez-Alcantara, O. Solorza-Feria, Electrochimica Acta 53 (2008) 4981.
[59] A.A. Abd-El-Latif, H. Baltruschat, Journal of Electroanalytical Chemistry 662 (2011) 204.
[60] H. Wang, H. Baltruschat, Journal of Physical Chemistry C 111 (2007) 7038.
[61] H. Wang, C. Wingender, H. Baltruschat, M. Lopez, M.T. Reetz, Journal of Electroanalytical Chemistry 509 (2001) 163.
[62] F. Maillard, E.R. Savinova, U. Stimming, Journal of Electroanalytical Chemistry 599 (2007) 221.
[63] S.C.S. Lai, N.P. Lebedeva, T.H.M. Housmans, M.T.M. Koper, Topics in Catalysis 46 (2007) 320.
[64] H. Liu, J. Zhang, Electrocatalysis of Direct Methanol Fuel Cells, WILEY-VCH Verlag GmbH & Co. KGaA, Weinheim, 2009.